Check for updates

Massive Natural Gas Hydrate Dissociation During the Penultimate Deglaciation (~130 ka) in the South China Sea

Jiangong Wei[1,2,3†], Tingting Wu[1,2†], Xiaoming Miao[4,5*] and Pibo Su[1,2,3,6*]

[1] Southern Marine Science and Engineering Guangdong Laboratory (Guangzhou), Guangzhou, China, [2] MLR Key Laboratory of Marine Mineral Resources, Guangzhou Marine Geological Survey, Guangzhou, China, [3] Academy of South China Sea Geological Science, China Geological Survey, Sanya, China, [4] College of Marine Geosciences, Ocean University of China, Qingdao, China, [5] Key Laboratory of Submarine Geosciences and Prospecting MOE China, Ocean University of China, Qingdao, China, [6] Hubei Key Laboratory of Marine Geological Resources, China University of Geosciences, Wuhan, China

There is widespread and growing scientific interest in the impact of massive gas hydrate dissociation on the global environment and climate in geological history. Based on that a global negative excursion of carbon isotopic compositions in marine (foraminifera) and terrestrial (the organic carbon and calcite) sedimentary records occurred during the penultimate deglaciation (~130 ka), we believe that methane released by hydrate dissociation may play a role in accelerating the initial increase of atmospheric methane. In order to prove that massive natural gas hydrate dissociation occurred in this period, we aim to seek for evidence of gas hydrate dissociation from seep carbonate. Here, X-ray diffraction, carbon and oxygen isotopic compositions, trace elements, and U-Th dating analyses were conducted on the deeply-buried authigenic carbonate obtained by drilling in the northern continental slope of the South China Sea. Authigenic carbonate formed at ~130 ka showed obvious characteristics of negative excursion of carbon isotope, positive excursion of oxygen isotope, and enrichment of redox sensitive elements such as Mo, U and As. These results, in particular the high oxygen isotopic compositions of carbonate, point to massive gas hydrate dissociation in the northern continental slope of the South China Sea during the penultimate deglaciation. It is further speculated that massive gas hydrate dissociation might have also occurred on a global scale, contributing to the increase of atmospheric carbon dioxide and methane concentrations during the penultimate deglaciation, and may eventually cause global carbon isotope negative excursion.

Keywords: the penultimate deglaciation, natural gas hydrate dissociation, seep carbonates, the South China Sea, anaerobic oxidation of methane

INTRODUCTION

There are huge reserves (1,000–10,000 Gt) of natural gas hydrate widely distributed in permafrost and continental margin sediments (Dickens et al., 1997). Changes in the sedimentary environment, such as temperature and sea level changes, can lead to the dissociation of natural gas hydrate and the release of methane (Crémière et al., 2016; Argentino et al., 2019; Chen et al., 2019; Deng et al., 2020). The release of these gasses can have an impact on the ocean, atmosphere, and even the global environment. Several major events that occurred in geological history may have been related to the massive gas hydrate dissociation, including the "Snowball Earth" termination event (Kennedy et al., 2008), the Permo-Triassic boundary (P/T) (Sluijs et al., 2007), the Early Toarcian oceanic anoxic event (OAE) during the Jurassic period (Hesselbo et al., 2000), the early Cretaceous (Jahren et al., 2001), the latest Palaeocene Thermal Maximum (LPTM) (Dickens et al., 1995; Dickens, 2001), and Quaternary Interstadials (Kennett et al., 2000; Dean et al., 2015).

Many marine and terrestrial sedimentary records of carbon isotopes indicate obvious negative excursion during the penultimate deglaciation (~130 ka). These records have been collected from regions such as the East Pacific (Shackleton and Hall, 1989), the Western Pacific (Schmidt et al., 1993), the northern Atlantic (Oppo et al., 1997), the South China Sea (Li and Wang, 2006), the Indian Ocean (Farrell and Janecek, 1991), Lake Baikal (Chappellaz et al., 1990), North America (Coplen et al., 1994), and Europe (Frogley et al., 1999). In addition, an ice core taken from Vostok recorded a rapid increase in global atmospheric methane and carbon dioxide levels during that time (Chappellaz et al., 1990), indicating the release of a large quantity of methane into the atmosphere during this period. Many people believe that the methane might originate from the increased vegetation (Coplen et al., 1994; Li and Wang, 2006; Häuselmann et al., 2015) or the extended wetlands, peatlands, and inundated floodplains (Chappellaz et al., 1990; Lourantou et al., 2010; Bock et al., 2017; Schmidely et al., 2021) in deglaciation times. However, most studies in recent years have shown that the release of methane from gas hydrates has a significant impact on climate change (Kennett et al., 2000; Shakhova et al., 2010; Berndt et al., 2014), including in polar regions (Serov et al., 2017) and other deep-sea areas (Reagan and Moridis, 2007; Foschi et al., 2020). Therefore, from the perspective of methane seepage, we believe that a large amount of methane from hydrate dissociation contributes to climate change. Some obvious directions of related future research include discussing the driver of negative excursion of global carbon isotopes, and identifying the link to the massive global dissociation of natural gas hydrate.

Previous studies have shown that the dissociation of natural gas hydrate will increase methane flux and further accelerate anaerobic oxidation of methane, thereby forming a large quantity of seep authigenic carbonate (Crémière et al., 2016; Feng et al., 2016; Lu et al., 2018; Argentino et al., 2019; Argentino et al., 2020; Lu et al., 2021). Sea-floor methane seepage leaves behind carbonate that have distinct geochemical signals that can be attributed to their origin (Svensen, 2012; Hu et al., 2014; Smrzka et al., 2020; Lin et al., 2021). Therefore, the hypothesis of massive

gas hydrate dissociation during ~130 ka can be tested by the study of cold-seep authigenic carbonate (Svensen, 2012). The South China Sea is considered a natural laboratory for the study of the dissociation and evolution of natural gas hydrate due to the extensive development of this resource in this region (Han et al., 2014; Feng et al., 2016; Wei et al., 2019; Ye et al., 2019; Miao et al., 2021a; Miao et al., 2021b; Miao et al., 2022). Here, the present study conducted X-ray diffraction, carbon and oxygen isotopic compositions, trace element, and U-Th dating analyses of authigenic carbonate obtained by drilling in the Qiongdongnan Basin of South China Sea (**Figure 1**). The aim of the present study was to identify regional evidence of massive gas hydrate dissociation during ~130 ka.

# MATERIALS AND METHODS

Materials
The GMGS5-W08 site was drilled to a depth of ~200 m below the seafloor (mbsf) at a water depth of ~1735 m in 2018 (Wei et al., 2019; Wei et al., 2020). And the bottom water temperature is ~3.5°C (Wei et al., 2019). A large number of gas hydrates were found in 54 mbsf, 63 mbsf, 64 mbsf and 69 mbsf and 70 mbsf (Wei et al., 2019). And continuous seep carbonate was discovered at the interval between 52–54 mbsf (Wei et al., 2020).

Methods
X-ray diffraction was used to analyze and identify the carbonate mineral composition. The samples were first dried for 7 h and then gently ground by a mortar. The ground sample was packed into X-ray sample holders for analysis. Scans were run at room temperature using a Rigaku SmartLab-9kW X-ray diffractometer with 8 kW power. The species and content of the minerals were analyzed by using the software PDXL2. The 2θ range is 3° to 75°, and speed of measurement is 7°/min. The voltage and current we used were 40 kV and 200 mA, respectively. In addition, the type of radiation we used was Cu.

Stable carbon and oxygen isotopic compositions were measured using a Thermo MAT-253 isotope ratio mass spectrometer. CO_2 gas was extracted by a reaction with supersaturated phosphoric acid on a Thermo Kiel IV Carbonate Device and was introduced into the MAT-253 dual inlet system. The isotope ratios were reported relative to Vienna Peedee Belemnite (VPDB). The precisions of $\delta^{13}C$ and $\delta^{18}O$ were ±0.1‰ and ±0.25‰, respectively.

For major and trace element content analysis, bulk seep carbonates were completely dissolved by HF and HNO_3 solutions following the procedure described in Hu et al. (2014). Briefly, ~50 mg sample was weighed and transferred into a pre-cleaned Teflon beaker followed by the addition of ultra-pure 1 ml of HF and 1 ml of HNO_3 solution. The beakers were then placed in steel cans and subjected to high temperature (185°C) and high pressure. After 36 h, the solution was dried on a hotplate. The residues were fully digested using a mixture of concentrated 2 ml HNO_3 and 3 ml Milli-Q water. Thereafter, the beakers were placed into steel cans at 120°C for 5 h. After cooling, the solution was diluted to 20 ml with Milli-Q water. Major elements were analysed with ICP-OES (Optima 8300, PerkinElmer, MA, USA),
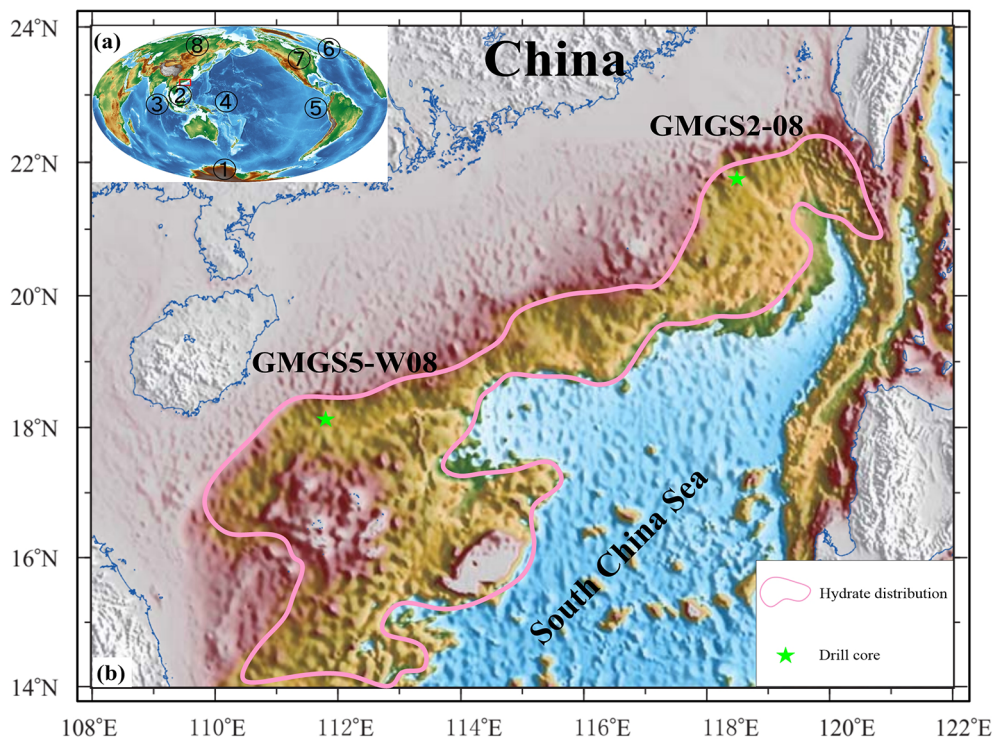
FIGURE 1 | (A) Map of earth showing regions containing marine and terrestrial sedimentary records of carbon isotopes indicating negative excursion during the penultimate deglaciation (~130 ka). The red rectangle represents the study area of the present study in the South China Sea; (1) represents the Vostok ice core (Chappellaz et al., 1990); (2) represents the South China Sea (Li and Wang, 2006); (3) represents the Indian Ocean (Farrell and Janecek, 1991); (4) represents the Western Pacific (Shackleton and Hall, 1989); (5) represents the Eastern Pacific (Schmidt et al., 1993); (6) represents the North Atlantic (Oppo et al., 1997); (7) represents North America (Coplen et al., 1994); (8) represents Lake Baikal (Prokopenko and Williams, 2004). **(B)** Map showing the study area of the present study located in the South China Sea.

and trace elements were measured *via* ICP-MS (X Series2, Thermo Fisher Scientific, MA, USA). The analytical precision was better than 5%.

The ^{230}Th dating work was performed at the Isotope Laboratory, Xi'an Jaiotong University using multi-collector inductively coupled plasma mass spectrometers (MC-ICP-MS) (Thermo-Finnigan Neptune-*plus*). We used standard chemistry procedures to separate U and Th for dating (Edwards et al., 1987). A triple-spike (^{229}Th–^{233}U–^{236}U) isotope dilution method was employed to correct for instrumental fractionation and determine U-Th isotopic ratios and concentrations. The instrumentation, standardization and half-lives are reported in *refs.* Cheng et al. (2000, 2013). All U-Th isotopes were measured on a MasCom multiplier behind the retarding potential quadrupole in the peak-jumping mode. We followed similar procedures of characterizing the multiplier as described in *ref.* Cheng et al. (2000). Uncertainties in U-Th isotopic data were calculated offline at 2σ level, including corrections for blanks, multiplier dark noise, abundance sensitivity, and contents of the same nuclides in spike solution. Corrected ^{230}Th ages assume the initial ^{230}Th/^{232}Th atomic ratio of $4.4 \pm 2.2 \times 10^{-6}$, the values for a material at secular equilibrium with the bulk earth ^{232}Th/^{238}U value of 3.8.

RESULTS

The carbonate content of GMGS5-W08 varied between 82.2%–100% (mean of 92.3%). Carbonates in the samples were mainly composed of aragonite (> 80 wt %) with minor amounts of calcite (**Table 1**).

The δ^{13}C values in the carbonate layers of GMGS5-W08 varied from −38.1‰ to −15.2‰, with mean values of −32.9‰ (n = 10) (**Figure 2** and **Table 2**). The δ^{18}O values in the carbonate layers of GMGS5-W08 ranged from 3.8‰ to 5.7‰, with mean values of 4.8‰ (n = 10) (**Figure 2** and **Table 2**).

Contents of major elements and trace elements in the bulk seep carbonates are presented in **Table 3**. In GMGS5-W08, Al content ranged from 0.09 to 3.97 wt. % (average 2.15 wt. %, n=16). U content ranged from 4.27 to 25.50 μg/g (average 16.99 μg/g, n=16). Th content ranged from 0.13 to 3.73 μg/g (average 2.66 μg/g, n=16). Mo content ranged from 4.06 to 52.74 μg/g (average 25.82 μg/g, n=16). V content ranged from 8.96 to 54.40 μg/g (average 36.20 μg/g, n=16). Ni content ranged from 3.66 to 83.38 μg/g (average 21.96 μg/g, n=16).

The enrichment factor (EF) was calculated as $X_{EF} = [(X/Al)_{sample}/(X/Al)_{PAAS}]$, where X and Al represent the weight concentrations of elements X and Al, respectively. The samples were normalized

TABLE 1 | Mineralogical compositions of seep carbonates.

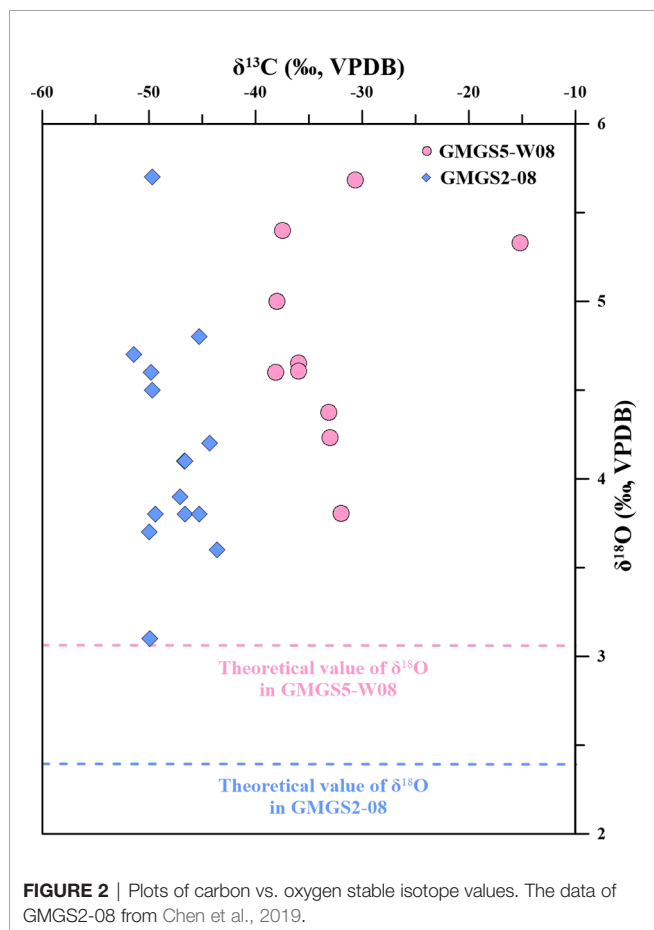| Core	Number	Depth (mbsf)	Mineral composition (%)					
			LMC	HMC	Aragonite	Dolomite	Quartz	Feldspar
GMGS5-W08	1	53.6	11.2		88.8			
	2	53.6	5.1		83.2		4.3	1.7
	3	53.6	11.8		79.2		5.0	0.8
	4	53.6	12.5		87.5			
	5	53.6	8.0		92.0			
	6	53.6		36.4	45.5	9.7	4.4	1.9
	7[a]	52.1	0.5		98.0			
	8[a]	52.1	4.2		80.5		11.2	0.6
	9[a]	53.6	3.9		84.0		8.9	1.2
	10[a]	53.6	2.4	2.2	83.8		9.6	1.2
	11[a]	53.6	3.3	1.9	83.1		8.7	0.6
	12[a]	53.6	8.7	1.9	83.1		3.3	0.6
	13[a]	53.6	3.8	2.0	88.0		5.1	
	14[a]	53.6	1.9		94.8		3.2	
	15[a]	53.6	5.8	35.9	40.5		9.8	1.4

LMC, low-magnesium calcite; HMC, high-magnesium calcite.
[a]*Data from (Wei et al. 2020).*

using the Post Archean Australian Shale (PAAS) composition (Taylor and McLennan, 1985). By calculation, the Mo enrichment factors (EF) in GMGS5-W08 seep carbonate vary from 56.4 to 2710.0 (average 278.9, n= 16) (**Figure 3A**). The

FIGURE 2 | Plots of carbon vs. oxygen stable isotope values. The data of GMGS2-08 from Chen et al., 2019.

U enrichment factors in GMGS5-W08 seep carbonate vary from 16.3 to 407.9 (average 53.1, n=16) (**Figure 3A**). The overall range of U/Th ratio is 5.08 to 86.87 (average 11.37, n= 16) (**Figure 3B**). The overall range of V/(V+Ni) ratio is 0.36 to 0.82 (average 0.63, n= 16) (**Figure 3C**).

Table 4 represents the U-Th ages of the three carbonate samples. The result showed that the ages of GMGS5-W08 (52–54mbsf) are 114.6 ± 0.5–136.3 ± 3.6 ka.

DISCUSSION

Fluid Sources and Formation Environments of Authigenic Carbonate

The carbon isotopic composition of authigenic carbonate can reveal the source of carbon during its formation, and the carbon isotopic composition is the most important indicator of methane-derived (Peckmann and Thiel, 2004; Lu et al., 2018; Deng et al., 2021; Lu et al., 2021). In general, seep carbonate shows obvious carbon isotope depletion, which is closely related to the anaerobic oxidation of methane (Peckmann and Thiel, 2004). The carbon isotopic ratios of the authigenic carbonate analyzed in the present study were relatively low, with the values of all samples, except for one, less than − 30‰ (**Figure 2** and **Table 2**). This is very similar to the cold seep carbonates from the site GMGS2-08 formed during ~ 130ka (Chen et al., 2019; Deng et al., 2021). These results indicate that the genesis of authigenic carbonate was related to methane seepage. However, the origin of methane reflected by methane carbon isotopes may vary. Among the samples, the carbon isotopic characteristics of carbonates from the site GMGS5-W08 were more similar to those of seep carbonates in the Gulf of Cadiz (Wang et al., 2015) and the Qiongdongnan Basin (Liang et al., 2017), and mainly of thermogenic or mixed origin. Carbonates in GMGS2-08 showed lower carbon isotopic ratios, indicating an apparent microbial methane component (Chen et al., 2019; Deng et al., 2021). Oxygen isotopes are

TABLE 2 | Carbon and oxygen isotopic ratios of seep carbonate layers.

Core	Number	Depth (mbsf)	$\delta^{13}C$ (‰, VPDB)	$\delta^{18}O$ (‰, VPDB)
GMGS5-W08	1 [a]	52.1	−38.0	5.0
	2	52.1	−30.6	5.7
	3 [a]	53.6	−36.0	4.7
	4	53.6	−35.9	4.6
	5	53.6	−32.0	3.8
	6	53.6	−15.2	5.3
	7	53.6	−33.1	4.4
	8	53.6	−33.0	4.2
	9	53.6	−38.1	4.6
	10	53.6	−37.5	5.4

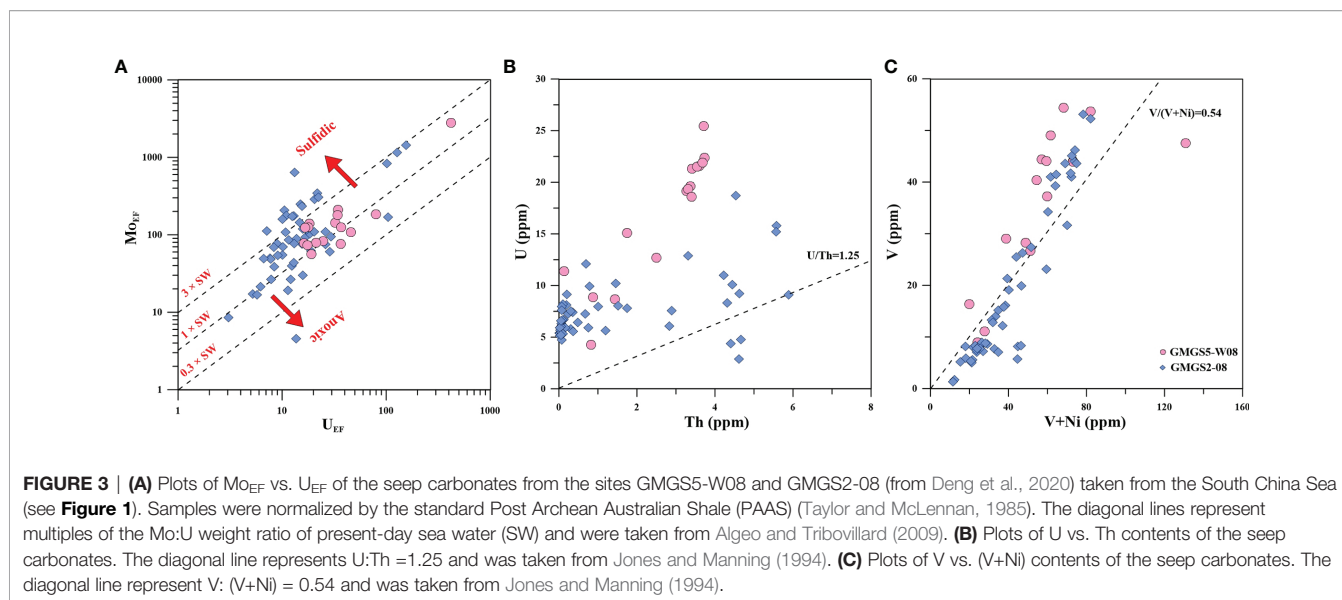[a]Data from (Wei et al. 2020).

mainly used to calculate equilibrium temperatures at the time of carbonate formation (Crémière et al., 2016). The present study used the oxygen isotopic fractionation equation of the aragonite water system by Kim et al. (2007) to calculate the expected equilibrium oxygen isotopic composition of aragonite. In this paper, we assume the bottom water temperature is 3.6 °C (Wei et al., 2019) and the $\delta^{18}O$ value of bottom water is 0‰ V-SMOW. The theoretical equilibrium values of oxygen isotopes of aragonite in GMGS5-W08 were 3.1‰ (**Figure 2**), higher than GMGS2-08 (2.4‰, Chen et al., 2019). In addition, the values of $\delta^{18}O$ of GMGS5-W08 exceeded the equilibrium theoretical values, showing characteristics of rich ^{18}O (**Figure 2**). This is very similar to other cold seep carbonates (Han et al., 2014; Feng and Chen, 2015; Crémière et al., 2016; Argentino et al., 2019) and is thought to be caused by ^{18}O-rich fluid of hydrate dissociation. During the period of ~130 ka, the oxygen isotope values recorded by foraminifera in the south China sea decreased significantly due to the increase of temperature (Li and Wang, 2006). Thus, the enrichment of ^{18}O in carbonate is influenced by fluids other than seawater. Two main sources of ^{18}O-rich fluids exist in the deep-sea sedimentary environment: (1) dehydration of clay minerals at greater depths (Hesse, 2003) and; (2) dissociation of natural gas hydrate (Chen et al., 2019). However, dehydration of clay

minerals is mainly caused by transformations between smectite and illite which require higher diagenetic temperature and pressure, and no significant smectite-illite mixtures have been found in the sediments. Therefore, dehydration of clay minerals may not be the main cause of heavy oxygen enrichment. However, the conditions of the South China Sea are favorable for the formation and development of natural gas hydrate (NGH). In fact, NGH was found in both GMGS5-W08 and GMGS2-08 (Chen et al., 2019; Wei et al., 2019). Therefore, the present study proposed that the generation of ^{18}O-rich fluid by dissociation of hydrate is the main driver of positive excursion of oxygen isotopes in the carbonate of the study area.

In addition to the stable carbon and oxygen isotopes compositions, the trace element composition of authigenic carbonate can be used to define the sedimentary environment and fluid geochemical characteristics at the time of their formation (Smrzka et al., 2020). A large amount of methane released from the dissociation of hydrate will accelerate the sulfate-driven anaerobic oxidation of methane (SD-AOM) (Peckmann and Thiel, 2004). Consequently, a large amount of H_2S will be released into pore water or even seawater, resulting in an environment in which carbonate deposition enters a reductive environment, thereby resulting in the enrichment of some trace elements (Hu et al., 2014; Smrzka et al., 2020). In our samples, we observed significant enrichment of Mo and U (**Figure 3A**). Previous studies have shown that the mechanisms responsible for U and Mo enrichment are different under anoxic conditions (Peketi et al., 2012; Sato et al., 2012). U tends to deposit in the Fe reduction zone, whereas Mo concentrates only in environments containing H_2S, and U is usually enriched earlier than Mo (Algeo and Tribovillard, 2009). However, the high methane fluxes will compress the suboxic and sulfidic zones into a narrow zone close to each other, resulting in the co-enrichment of Mo and U (Chen et al., 2016; Miao et al., 2021a; Miao et al., 2022). Therefore, the co-enrichment of Mo and U in methane seepage environment is very common and has been widely used to reconstruct carbonate formation environments (Deng et al., 2020; Smrzka et al., 2020),

TABLE 3 | Major and trace element contents of seep carbonates.

Core	Number	Depth	Al	Fe	Mn	Cu	Zn	U	Th	Mo	V	Ni	As
		(mbsf)	(wt.%)					(µg/g)					
GMGS5-W08	1	52.1	0.09	–	0.012	10.2	27.55	11.38	0.131	24.39	8.961	15.17	3.02
	2	52.1	3.81	0.95	0.034	20.76	57.5	21.58	3.604	52.74	44.08	29.01	6.64
	3	52.1	2.00	0.90	0.075	17.6	37.2	22.40	3.73	14.90	54.40	13.90	–
	4	52.1	0.40	0.16	0.017	5.27	10.4	8.87	0.88	6.63	16.40	3.66	–
	5	52.1	1.80	0.83	0.076	11.8	36.3	25.50	3.71	19.5	49.1	12.5	–
	6	53.6	1.96	0.23	0.028	13.3	36.18	15.09	1.752	16.29	28.25	20.59	3.53
	7	53.6	3.86	1.15	0.037	17.45	53.02	21.3	3.416	47.97	47.52	83.38	6.76
	8	53.6	3.89	0.88	0.034	17.11	51.29	19.62	3.369	30.27	53.67	28.49	6.20
	9	53.6	3.72	1.02	0.041	16.57	50.84	19.13	3.268	45.53	43.94	29.07	6.69
	10	53.6	0.72	–	0.016	9.685	27.62	4.274	0.822	4.056	11.06	16.69	4.58
	11	53.6	1.33	0.03	0.019	14.72	41.26	8.68	1.441	10.41	26.67	24.59	4.05
	12	53.6	3.97	0.92	0.064	14.86	47.30	21.50	3.538	29.15	37.23	22.61	3.47
	13	53.6	1.30	0.68	0.091	7.63	22.30	12.70	2.50	17.93	29.07	9.65	–
	14	53.6	1.90	0.91	0.148	10.50	30.10	21.90	3.68	23.84	44.35	12.70	–
	15	53.6	1.80	1.05	0.114	10.50	31.30	19.30	3.32	38.16	44.07	15.30	–
	16	53.6	1.80	0.97	0.135	10.40	31.50	18.60	3.40	31.38	40.35	14.10	–

FIGURE 3 | (A) Plots of Mo$_{EF}$ vs. U$_{EF}$ of the seep carbonates from the sites GMGS5-W08 and GMGS2-08 (from Deng et al., 2020) taken from the South China Sea (see **Figure 1**). Samples were normalized by the standard Post Archean Australian Shale (PAAS) (Taylor and McLennan, 1985). The diagonal lines represent multiples of the Mo:U weight ratio of present-day sea water (SW) and were taken from Algeo and Tribovillard (2009). (B) Plots of U vs. Th contents of the seep carbonates. The diagonal line represents U:Th =1.25 and was taken from Jones and Manning (1994). (C) Plots of V vs. (V+Ni) contents of the seep carbonates. The diagonal line represent V: (V+Ni) = 0.54 and was taken from Jones and Manning (1994).

such as the South China Sea (Lin et al., 2021; Miao et al., 2021a) and northern Apennines (Argentino et al., 2019). As shown in **Figure 4A**, the carbonates of GMGS5-W08 and GMGS2-08 exhibit similar geochemical characteristics. Mo$_{EF}$ of carbonates in the study area was significantly greater than U$_{EF}$, and the Mo$_{EF}$/U$_{EF}$ ratio of GMGS5-W08 ranges from 2.1 to 7.6. In addition, plotted in the Mo$_{EF}$ vs. U$_{EF}$ diagram, they mostly fall in > 0.3×(Mo/U)$_{SW}$ trend lines, indicating that the carbonates were formed in an anoxic environment or even sulfidic environment (Chen et al., 2016; Argentino et al., 2019). At the same time, the ratios of U/Th (> 1.25) and V/(V+Ni) (> 0.54) of seep carbonates also supports this view (**Figures 3B, C**) (Jones and Manning, 1994; Wignall and Twitchett, 1996).

In addition, organic matter, iron, and manganese oxides are potential hosts for Mo in the sediments (Algeo and Tribovillard, 2009; Scholz et al., 2011). Mo enrichment is usually evident in organic-rich sediments at modern continental margins (Scholz et al., 2011). However, in this sample, other redox sensitive elements (e.g., Ni, Cu, and Zn) that are associated with organic

matter are not enriched (**Table 3**), which is obviously different from organic-rich sediments (Scholz et al., 2011). At the same time, the extremely low Mn content (average value was 0.059%) and anoxic environment (U/Th > 1.25 and V/(V+Ni) > 0.54) indicate that the content of Mn oxides in carbonate hardly exists. Therefore, Mo enrichment has little relation with organic matter and Fe and Mn oxides (Smrzka et al., 2020). And, considering comprehensively the characteristics of authigenic carbonate, the current study proposed that the formation process of authigenic carbonate in the study area is mainly controlled by the dissociation of hydrate.

Interestingly, arsenic (As) in the the carbonates of GMGS5-W08 and GMGS2-08 (Deng et al., 2020) has obvious enrichment characteristics (**Figure 4**, 0.1 to 179.8, the mean value was 20.4). This phenomenon is also common in cold-seep environments and is often used to determine the source of Mo (Hu et al., 2014; Argentino et al., 2019; Lin et al., 2021; Miao et al., 2022). The particulate shuttle process is one of the reasons for the common enrichment of Mo and As (Algeo and Tribovillard, 2009;

TABLE 4 | U-Th isotopic data and calculated ages of seep carbonates.

Core	Depth(mbsf)	^{238}U	^{232}Th	^{230}Th/^{232}Th	δ^{234}U[a]	^{230}Th/^{238}U	^{230}Th Age (ka BP)	^{230}Th Age (ka BP)[b]	δ^{234}U$_{Initial}$[c]
		(ppb)	(ppt)	(atomic × 10^{-6})	(measured)	(activity)	(uncorrected)	(corrected)	(corrected)
GMGS5-W08	52.1[d]	22064 ± 121	3207882 ± 67017	92.9 ± 2.0	112.9 ± 3.9	0.1512 ± 0.0013	136.3 ± 3.6	136.3 ± 3.6	166 ± 6
	53.6[d]	14674 ± 51	1886966 ± 38243	113.9 ± 2.3	101.1 ± 2.4	0.7913 ± 0.0037	131.1 ± 2.5	131.1 ± 2.5	146 ± 4
	53.6	8828 ± 12	138481± 2776	756 ± 15	90.1 ± 1.2	0.7190 ± 0.0014	115.0 ± 0.5	114.6 ± 0.5	124 ± 2

U decay constants: λ$_{238}$ = 1.55125 × 10^{-10} (Jaffey et al., 1971) and λ$_{234}$ = 2.82206 × 10^{-6} (Cheng et al., 2013). Th decay constant: λ$_{230}$ = 9.1705 × 10^{-6} (Cheng et al., 2013). Corrected ^{230}Th ages assume the initial ^{230}Th/^{232}Th atomic ratio of 4.4 ± 2.2 × 10^{-6}. Those are the values for a material at secular equilibrium, with the bulk earth ^{232}Th/^{238}U value of 3.8. The errors are arbitrarily assumed to be 50%.
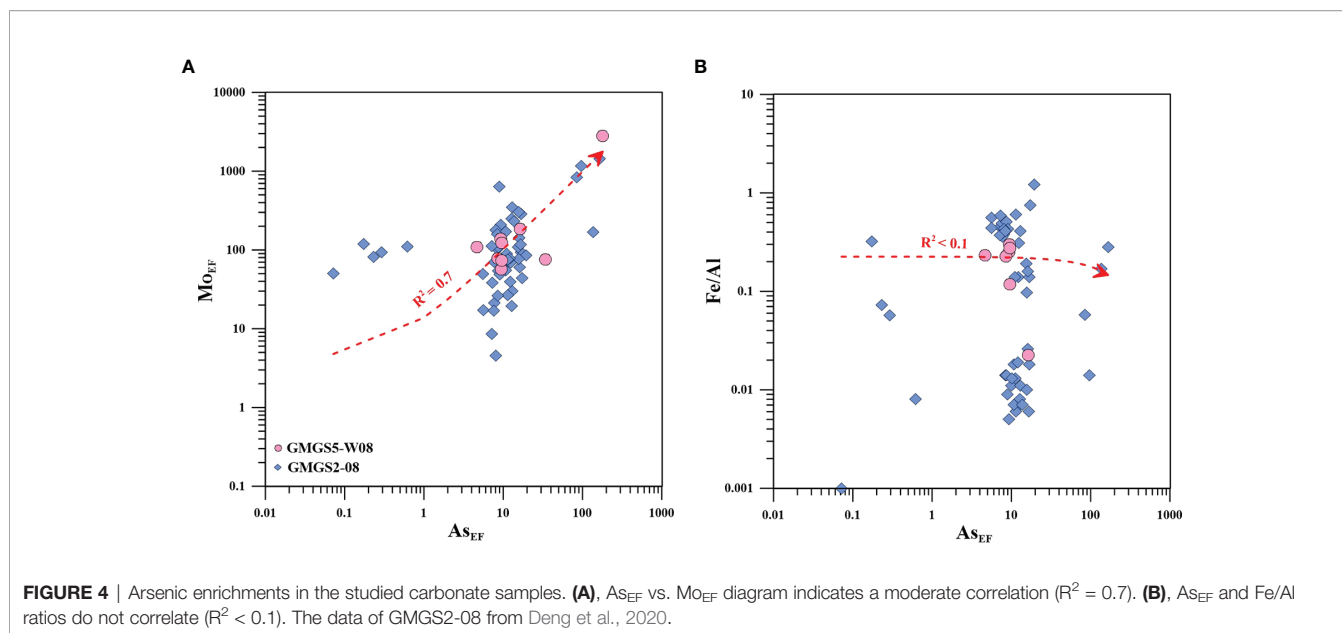*The uncertainties of our age data are quoted at 2σ.*
[a]δ^{234}U = ([^{234}U/^{238}U]$_{activity}$ − 1) × 1000.
[b]B.P. stands for "Before Present" where the "Present" is defined as the year 1950 A.D.
[c]δ^{234}U$_{initial}$ was calculated based on ^{230}Th age (T), i.e., δ^{234}U$_{initial}$ = δ^{234}U$_{measured}$ × e$^{λ234 × T}$.
[d]Data from Wei et al. (2020).

FIGURE 4 | Arsenic enrichments in the studied carbonate samples. (A), As_{EF} vs. Mo_{EF} diagram indicates a moderate correlation ($R^2 = 0.7$). (B), As_{EF} and Fe/Al ratios do not correlate ($R^2 < 0.1$). The data of GMGS2-08 from Deng et al., 2020.
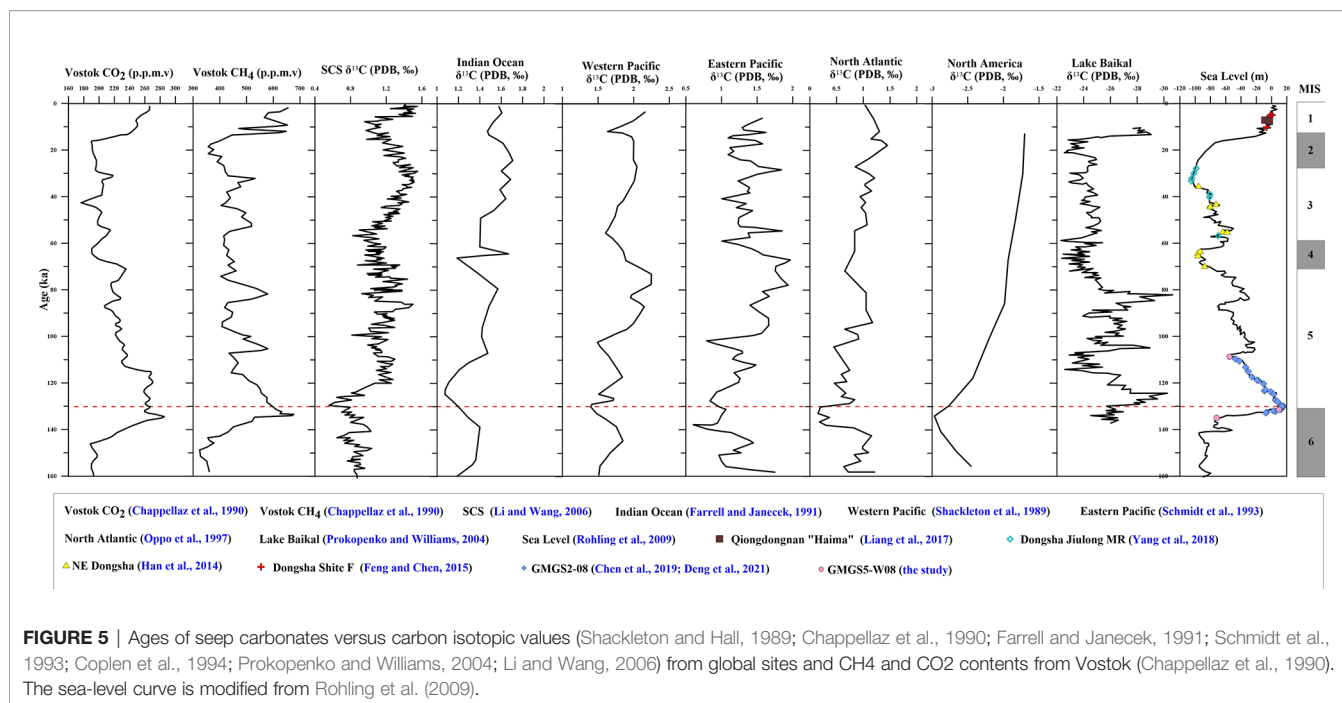
Scott and Lyons, 2012). Iron and manganese (hydrogen) oxides can remove trace elements from water and then transfer to surface sediments (Smrzka et al., 2020). Subsequently, in the sulfidic environment, the adsorbed trace elements are released into the pore water, which is eventually scavenged again by authigenic iron sulfide minerals (Hu et al., 2014; Scholz et al., 2017). In our study, although As_{EF} and Mo_{EF} has a very high positive correlation (**Figure 4**, $R^2 = 0.7$), the correlation between the As_{EF} and the ratio of Fe/Al is very low (**Figure 4**, $R^2 < 0.1$). Obviously, particulate shuttle process is not the main factor controlling Mo and As enrichment. However, the common enrichment of Mo and U in carbonate indicates an overlap or at least a close proximity of the iron reduction zone and the sulfate-methane transition zones (SMTZ). Moreover, combined with bivalve shells in the samples (Wei et al., 2020; Deng et al., 2021), we believe that methane seepage is strong and SMTZ is formed at or near the seafloor. As a result, We suggest that Mo fixation in authigenic iron sulfide can be enhanced by seeps at shallow SMTZs, with seawater being the main source of Mo (Peketi et al., 2012; Lin et al., 2021).

Significance of Cold Seep Activity During the Penultimate Deglaciation (~130 ka)

U-Th dating of cold seep carbonate is of great significance for determining the age of dissociation of natural gas hydrates (Crémière et al., 2016; Chen et al., 2019). The results of U-Th dating in the current study showed that although the seep carbonates in the areas of hydrate occurrence in the South China Sea are buried in different sedimentary horizons, they were formed at roughly the same time, i.e., during the penultimate deglaciation (~130 ka) (**Figure 5** and **Table 4**). According to the seismic reflection profiles of GMGS5-W08, the authigenic carbonate sample at 52-54 mbsf coincides with a high-amplitude reflector at 54 mbsf that extends laterally over 4500 m, which suggests that the carbonate concretions were

developed not only within the gas chimney but across the paleo-seafloor (Ye et al., 2019). In addition, the Dongsha area in the South China Sea has also found cold seep carbonates formed at ~130ka (Chen et al., 2019; Deng et al., 2021). This result confirms that a massive gas hydrate dissociation event occurred in the northern continental slope of the South China Sea during this period.

In general, the pressure change caused by sea level fall and temperature change caused by bottom water temperature rise are the main factors that trigger hydrate dissociation in continental margin (Kennett et al., 2000; Shakhova et al., 2010; Dean et al., 2015; Deng et al., 2021). In **Figure 5**, we find that the carbonates were mainly formed in MIS6/5e. During the MIS6/5e transition period, the sea level was higher than the modern sea level (Rohling et al., 2009), which increased the stability of seabed hydrate and inhibited the dissociation of hydrate. Therefore, sea level change was not the main factor of hydrate dissociation during this period. However, Chen et al. (2019) found that the bottom water temperature of the South China Sea increased by 1.8-4.5°C during this period, which was enough to trigger the dissociation of hydrate. Because every 1°C increase in the temperature of bottom water is enough to trigger the dissociation of local hydrates (Reagan and Moridis, 2007). Therefore, we believe that the dissociation of hydrate in this period was caused by the rise of bottom water temperature. During the transition from glacial to interglacial, the temperature of bottom water increased in almost all sea areas (Rohling et al., 2014). For example, during deglaciation, the temperature of the bottom water in the Atlantic increased by 3- 4.5°C (Dwyer et al., 1995). Therefore, we believe that hydrate dissociation may also occur in other hydrate regions around the world. In Bock et al. (2017), when the concentration of CH_4 starts to increase at the initial stage of the penultimate deglaciation, the δD and $\delta^{13}C$ values of CH_4 are also increased slightly. Such synchronous variations may indicate methane source from gas hydrate dissociation. This result

FIGURE 5 | Ages of seep carbonates versus carbon isotopic values (Shackleton and Hall, 1989; Chappellaz et al., 1990; Farrell and Janecek, 1991; Schmidt et al., 1993; Coplen et al., 1994; Prokopenko and Williams, 2004; Li and Wang, 2006) from global sites and CH4 and CO2 contents from Vostok (Chappellaz et al., 1990). The sea-level curve is modified from Rohling et al. (2009).

combined with the observed negative excursion of global carbon isotopes and the rapid increase in CH_4 content in the atmosphere during this period (**Figure 5**) indicates that the hydrate dissociation event during the penultimate deglaciation period (~130 ka) may have occurred at a global scale. According to " The Clathrate Gun Hypothesis " hypothesis (Kennett et al., 2003), we believe that this event may be one of the driver of the global negative excursion of carbon isotopes and the increase in atmospheric methane and carbon dioxide content. Throughout the late Pleistocene, we find that this phenomenon is quite common. Hydrate dissociation events occurred in MIS10/9 (Tong et al., 2013), MIS4/3 (Han et al., 2014; Yang et al., 2018) and MIS2/1 (Wei et al., 2020; Deng et al., 2021) periods.

In addition, age of carbonate (114.6–136.3ka) indicate that methane seepage occurred not only during MIS6/5e, but throughout MIS5e (**Figure 5**). Methane is a very important greenhouse gas, and its increase in the atmosphere is bound to cause global warming (Hesselbo et al., 2000; Kennett et al., 2000). At the same time, we believe that the climate warming caused by the continuous release of methane may be one of the reasons for maintaining the temperature of interglacial and delaying the arrival of glacial.

CONCLUSION AND OUTLOOK

The geochemical characteristics and U-Th dating of deep authigenic carbonate in different areas of the South China Sea provide strong evidence for a massive gas hydrate dissociation event during the penultimate deglaciation (~130 ka). Although the present study focused on carbonate in the South China Sea,

this phenomenon should also exist in the seeping hydrates of other marine areas worldwide, which should be confirmed by future studies. At the same time, the current study proposes that the massive gas hydrate dissociation during this period was related to changes relating to the glacial-interglacial period. The rise of sea water temperature that occurred at the end of the glacial period and beginning of the interglacial period was the main driver of the dissociation of hydrate (Chen et al., 2019; Deng et al., 2021). Moreover, large amounts of methane released by hydrate decomposition may have entered the ocean and atmosphere, which would have contributed positively to the sudden warming of the climate during the penultimate deglaciation.

DATA AVAILABILITY STATEMENT

The original contributions presented in the study are included in the article/supplementary material. Further inquiries can be directed to the corresponding authors.

AUTHOR CONTRIBUTIONS

JW collected samples. XM formal analysis. JW, TW, XM, and PS writing–review and editing. PS and JW funding acquisition. JW and TW wrote the paper with contributions from all the co-authors. All authors contributed to the article and approved the submitted version.

FUNDING

REFERENCES

Algeo, T., and Tribovillard, N. (2009). Environmental Analysis of Paleoceanographic Systems Based on Molybdenum Uranium Covariation. *Chem. Geol.* 268, 211–225. doi: 10.1016/j.chemgeo.2009.09.001

Argentino, C., Johnson, J. E., Conti, S., Fioroni, C., and Fontana, D. (2020). Preservation of 34S-Enriched Sulfides in Fossil Sulfate-Methane Transition Zones: New Evidence From Miocene Outcrops of the Northern Apennines (Italy). *Geo Marine Lett.* 40, 379–390. doi: 10.1007/s00367-020-00644-w

Argentino, C., Lugli, F., Cipriani, A., Conti, S., and Fontana, D. (2019). A Deep Fluid Source of Radiogenic Sr and Highly Dynamic Seepage Conditions Recorded in Miocene Seep Carbonates of the Northern Apennines (Italy). *Chem. Geol.* 522, 135–147. doi: 10.1016/j.chemgeo.2019.05.029

Berndt, C., Feseker, T., Treude, T., Krastel, S., Lieberau, V., Niemann, H., et al. (2014). Temporal Constraints on Hydrate-Controlled Methane Seepage Off Svalbard. *Science* 343, 284–287. doi: 10.1126/science.1246298

Bock, M., Schmitt, J., Beck, J., Seth, B., Chappellaz, J., and Fischer, H. (2017). Glacial/interglacial Wetland, Biomass Burning, and Geologic Methane Emissions Constrained by Dual Stable Isotopic CH4 Ice Core Records. *Proc. Natl. Acad. Sci. U. S. A.* 114 (29), E5778. doi: 10.1073/pnas.1613883114

Chappellaz, J., Barnola, J. M., Raynaud, D., Korotkevich, Y. S., and Lorius, C. (1990). Ice-Core Record of Atmospheric Methane Over the Past 160,000 Years. *Nature* 345, 127–131. doi: 10.1038/345127a0

Cheng, H., Edwards, R. L., Hoff, J., Gallup, C. D., Richards, D. A., and Asmerom, Y. (2000). The Half-Lives of U-234 and Th-230. *Chem. Geol.* 169, 17–33. doi: 10.1016/S0009-2541(99)00157-6

Cheng, H., Edwards, R. L., Shen, C.–C., Polyak, V. J., Asmerom, Y., Woodhead, J., et al. (2013). Improvements in 230Th Dating, 230Th and 234U Half-Life Values, and U–Th Isotopic Measurements by Multi-Collector Inductively Coupled Plasma Mass Spectrometry. *Earth Planet. Sc. Lett.* 371, 82–91. doi: 10.1016/j.epsl.2013.04.006

Chen, F., Hu, Y., Feng, D., Zhang, X., Cheng, S., Gao, J., et al. (2016). Evidence of Intense Methane Seepages From Molybdenum Enrichments in Gas Hydrate-Bearing Sediments of the Northern South China Sea. *Chem. Geol.* 443, 173–181. doi: 10.1016/j.chemgeo.2016.09.029

Chen, F., Wang, X., Li, N., Cao, J., Bayon, G., Peckmann, J., et al. (2019). Gas Hydrate Dissociation During Sea-Level Highstand Inferred From U/Th Dating of Seep Carbonate From the South China Sea. *Geophys. Res. Lett.* 46, 13928–13938. doi: 10.1029/2019GL085643

Coplen, T. B., Winograd, I. J., Landwehr, J. M., and Riggs, A. C. (1994). 500,000-Year Stable Carbon Isotopic Record From Devils Hole, Nevada. *Science* 263, 361–365. doi: 10.1126/science.263.5145.361

Crémière, A., Lepland, A., Chand, S., Sahy, D., Condon, D. J., Noble, S. R., et al. (2016). Timescales of Methane Seepage on the Norwegian Margin Following Collapse of the Scandinavian Ice Sheet. *Nat. Commun.* 7, 11509. doi: 10.1038/ncomms11509

Dean, W. E., Kennett, J. P., Behl, R. J., Nicholson, C., and Sorlien, C. C. (2015). Abrupt Termination of Marine Isotope Stage 16 (Termination VII) at 631.5 Ka in Santa Barbara Basin, California. *Paleoceanography* 30, 1373–1390. doi: 10.1002/2014PA002756

Deng, Y., Chen, F., Guo, Q., Hu, Y., Chen, D., Yang, S., et al. (2021). Possible Links Between Methane Seepages and Glacial-Interglacial Transitions in the South China Sea. *Geophys. Res. Lett.* 48, e2020GL091429. doi: 10.1029/2020GL091429

Deng, Y., Chen, F., Hu, Y., Guo, Q., Cao, J., Chen, H., et al. (2020). Methane Seepage Patterns During the Middle Pleistocene Inferred From Molybdenum Enrichments of Seep Carbonates in the South China Sea. *Ore Geol. Rev.* 125, 103701. doi: 10.1016/j.oregeorev.2020.103701

Dickens, G. R. (2001). Modeling the Global Carbon Cycle With a Gas Hydrate Capacitor: Significance for the Latest Paleocene Thermal Maximum. *Am. Geophys. Union.* 124, 19–38. doi: 10.1029/GM124p0019

Dickens, G. R., Castillo, M. M., and Walker, J. C. G. (1997). A Blast of Gas in the Latest Paleocene: Simulating First-Order Effects of Massive Dissociation of Oceanic Methane Hydrate. *Geology* 25, 259–262. doi: 10.1130/0091-7613(1997)025<0259:ABOGIT>2.3.CO;2

Dickens, G. R., O'Neil, J. R., Rea, D. K., and Owen, R. M. (1995). Dissociation of Oceanic Methane Hydrate as a Cause of the Carbon Isotope Excursion at the End of the Paleocene. *Paleoceanography* 10, 965–971. doi: 10.1029/95PA02087

Dwyer, G. S., Cronin, T. M., Baker, P. A., Raymo, M. E., Buzas, J. S., and Corrège, T. (1995). North Atlantic Deepwater Temperature Change During Late Pliocene and Late Quaternary Climatic Cycles. *Science* 270, 1347–1351. doi: 10.1126/science.270.5240.1347

Edwards, R. L., Chen, J. H., and Wasserburg, G. J. (1987). 238U, 234U, 230Th, 232Th Systematics and the Precise Measurement of Time Over the Past 500,000 Years. *Earth Planet. Sc. Lett.* 81, 175–192. doi: 10.1016/0012-821X(87)90154-3

Farrell, J. W., and Janecek, T. R. (1991). Late Neogene Paleoceanography and Paleoclimatology of the Northeast Indian Ocean (Site 758). *Ocean Drill. Prog. Sci. Results.* 121, 297–355. doi: 10.2973/odp.proc.sr.121.124.1991

Feng, D., and Chen, D. (2015). Authigenic Carbonates From an Active Cold Seep of the Northern South China Sea: New Insights Into Fluid Sources and Past Seepage Activity. *Dee Sea Res. Pt. II.* 122, 74–83. doi: 10.1016/j.dsr2.2015.02.003

Feng, D., Peng, Y. B., Bao, H. M., Peckmann, J., Roberts, H. H., and Chen, D. F. (2016). A Carbonate-Based Proxy For Sulfate-Driven Anaerobic Oxidation of Methane. *Geology* 44, 999–1002. doi: 10.1130/G38233.1

Foschi, M., Cartwright, J., Macminn, C. W., and Etiope, G. (2020). Evidence for Massive Emission of Methane From a Deep-Water Gas Field During the Pliocene. *P. Natl. Acad. Sci.* 117 (45), 27869–27876. doi: 10.1073/pnas.2001904117

Frogley, M. R., Tzedakis, P. C., and Heaton, T. H. E. (1999). Climate Variability in Northwest Greece During the Last Interglacial. *Science* 285, 1886–1889. doi: 10.1126/science.285.5435.1886

Han, X., Suess, E., Liebetrau, V., Eisenhauer, A., and Huang, Y. (2014). Past Methane Release Events and Environmental Conditions at the Upper Continental Slope of the South China Sea: Constraints by Seep Carbonates. *Int. J. Earth Sci.* 103, 1873–1887. doi: 10.1007/s00531-014-1018-5

Häuselmann, A. D., Fleitmann, D., Cheng, H., Tabersky, D., Gunther, D., Edwards, R. L., et al. (2015). Timing Andnature of the Penultimate Deglaciation in a High Alpine Stalagmitefrom Switzerland. *Quaternary Sci. Rev.* 126, 264 275. doi: 10.1016/j.quascirev.2015.08.026

Hesse, R. (2003). Pore Water Anomalies of Submarine Gas-Hydrate Zones as Tool to Assess Hydrate Abundance and Distribution in the Subsurface. *Earth Sci. Rev.* 61, 149–179. doi: 10.1016/S0012-8252(02)00117-4

Hesselbo, S. P., Grocke, D. R., Jenkyns, H. C., Bjerrum, C. J., Farrimond, P., Morgans, B., et al. (2000). Massive Dissociation of Gas Hydrate During a Jurassic Oceanic Anoxic Event. *Nature* 406, 392–395. doi: 10.1038/35019044

Hu, Y., Feng, D., Peckmann, J., Roberts, H. H., and Chen, D. (2014). New Insights Into Cerium Anomalies and Mechanisms of Trace Metal Enrichment in Authigenic Carbonate From Hydrocarbon Seeps. *Chem. Geol.* 381, 55–66. doi: 10.1016/j.chemgeo.2014.05.014

Jaffey, A. H., Flynn, K. F., Glendenin, L. E., Bentley, W. C., and Essling, A. M. (1971). Precision Measurement of Half-Lives and Specific Activities of ^{235}U and ^{238}U. *Phys. Rev. C.* 4, 1889–1906. doi: 10.1103/PhysRevC.4.1889

Jahren, A. H., Arens, N. C., Sarmiento, G., Guerrero, J., and Amundson, R. (2001). Terrestrial Record of Methane Hydrate Dissociation in the Early Cretaceous. *Geology* 29, 159–162. doi: 10.1130/0091-7613(2001)029<0159:TROMHD>2.0.CO;2

Jones, B. J., and Manning, A. C. (1994). Comparison of Geochemical Indices Used for the Interpretation of Palaeoredox Conditions in Ancient Mudstones. *Chem. Geol.* 111, 111–129. doi: 10.1016/0009-2541(94)90085-X

Kennedy, M., Mrofka, D., and Borch, C. (2008). Snowball Earth Termination by Destabilization of Equatorial Permafrost Methane Clathrate. *Nature* 453, 642–645. doi: 10.1038/nature06961

Kennett, J. P., Cannariato, K. G., Hendy, I. L., and Behl, R. (2000). Carbon Isotopic Evidence for Methane Hydrate Instability During Quaternary Interstadials. *Science* 288, 128–133. doi: 10.1126/science.288.5463.128

Kennett, J. P., Cannariato, K. G., Hendy, I. L., and Behl, R. J. (2003). *Methane Hydrates in Quaternary Climate Change: The Clathrate Gun Hypothesis* Vol. 216 (AGU, Washington, D. C: American Geophysical Union).

Kim, S. T., O'Neil, J. R., Hillaire Marcel, C., and Mucci, A. (2007). Oxygen Isotope Fractionation Between Synthetic Aragonite and Water: Influence of Temperature and Mg2+ Concentration. *Geochim. Cosmochim. Ac.* 71, 4704–4715. doi: 10.1016/j.gca.2007.04.019

Liang, Q. Y., Hu, Y., Feng, D., Peckmann, J., Chen, L., Yang, S., et al. (2017). Authigenic Carbonates From Newly Discovered Active Cold Seeps on the Northwestern Slope of the South China Sea: Constraints on Fluid Sources, Formation Environments, and Seepage Dynamics. *Dee Sea Res. I.* 124, 31–41. doi: 10.1016/j.dsr.2017.04.015

Lin, Z., Sun, X., Strauss, H., Eroglu, S., Bo¨ttcher, M. E., Lu, Y., et al. (2021). Molybdenum Isotope Composition of Seep Carbonates – Constraints on Sediment Biogeochemistry in Seepage Environments. *Geochim. Cosmochim. Ac.* 307, 56–71. doi: 10.1016/j.gca.2021.05.038

Li, J., and Wang, P. (2006). Carbon Isotope Record of 200 Kyr in the South China Sea. *Chin. Sci. Bull.* 51, 1482–1486. doi: 10.1007/s11434-006-2032-1

Lourantou, A., Chappellaz, J., Barnola, J. M., Delmotte, V. M., and Raynaud, D. (2010). Changes in Atmospheric CO2 and its Carbon Isotopic Ratio During the Penultimate Deglaciation. *Quaternary Sci. Rev.* 29 (17-18), 1983–1992. doi: 10.1016/j.quascirev.2010.05.002

Lu, Y., Sun, X., Xu, H., Konishi, H., Lin, Z., Xu, L., et al. (2018). Formation of Dolomite Catalyzed by Sulfate-Driven Anaerobic Oxidation of Methane: Mineralogical and Geochemical Evidence From the Northern South China Sea. *Am. Mineralogist* 103 (5), 720–734. doi: 10.2138/am-2018-6226

Lu, Y., Yang, X., Lin, Z., Sun, X., Yang, Y., and Peckmann, J. (2021). Reducing Microenvironments Promote Incorporation of Magnesium Ions Into Authigenic Carbonate Forming at Methane Seeps: Constraints for Dolomite Formation. *Sedimentology* 68, 2945–2964. doi: 10.1111/sed.12919

Miao, X., Feng, X., Li, J., and Lin, L. (2021a). Tracing the Paleo-Methane Seepage Activity Over the Past 20,000years in the Sediments of Qiongdongnan Basin, Northwestern South China Sea. *Chem. Geol.* 559, 119956. doi: 10.1016/j.chemgeo.2020.119956

Miao, X., Feng, X., Li, J., Liu, X., Liang, J., Feng, J., et al. (2022). Enrichment Mechanism of Trace Elements in Pyrite Under Methane Seepage. *Geochem. Persp. Let.* 21, 18–22. doi: 10.7185/geochemlet.2211

Miao, X., Feng, X., Liu, X., Li, J., and Wei, J. (2021b). Effects of Methane Seepage Activity on the Morphology and Geochemistry of Authigenic Pyrite. *Mar. Petrol. Geol.* 133, 105231. doi: 10.1016/j.marpetgeo.2021.105231

Oppo, D. W., Horowitz, M., and Lehman, S. J. (1997). Marine Core Evidence for Reduced Deepwater Production During Termination Followed by a Relatively Stable Substage 5e (Eemian). *Paleoceanography* 12, 51–63. doi: 10.1029/96PA03133

Peckmann, J., and Thiel, V. (2004). Carbon Cycling at Ancient Methane–Seeps. *Chem. Geol.* 205, 443–467. doi: 10.1016/j.chemgeo.2003.12.025

Peketi, A., Mazumdar, A., Joshi, R. K., Patil, D. J., Srinivas, P. L., and Dayal, A. M. (2012). Tracing the Paleo Sulfate-Methane Transition Zones and H2S Seepage Events in Marine Sediments: An Application of C-S-Mo Systematics. *Geochem. Geophy. Geosy.* 13 (10). doi: 10.1029/2012GC004288

Prokopenko, A. A., and Williams, D. F. (2004). Deglacial Methane Emission Signals in the Carbon Isotopic Record of Lake Baikal. *Earth Planet. Sci. Lett.* 218 (1), 135–147. doi: 10.1016/S0012-821X(03)00637-X

Reagan, M. T., and Moridis, G. J. (2007). Oceanic Gas Hydrate Instability and Dissociation Under Climate Change Scenarios. *Geophys. Res. Lett.* 34, L22709. doi: 10.1029/2007GL031671

Rohling, E. J., Foster, G. L., Grant, K. M., Marino, G., Roberts, A. P., Tamisiea, M. E., et al. (2014). Sea-Level and Deep-Sea-Temperature Variability Over the Past 5.3 Million Years. *Nature* 508, 477–482. doi: 10.1038/nature13230

Rohling, E. J., Grant, K., Bolshaw, M., Roberts, A. P., Siddall, M., Hemleben, C., et al. (2009). Antarctic Temperature and Global Sea Level Closely Coupled Over the Past Five Glacial Cycles. *Nat. Geosci.* 2, 500–504. doi: 10.1038/ngeo557

Sato, H., Hayashi, K., Ogawa, Y., and Kawamura, K. (2012). Geochemistry of Deep Sea Sediments at Cold Seep Sites in the Nankai Trough: Insights Into the Effect of Anaerobic Oxidation of Methane. *Mar. Geol.* 323, 47–55. doi: 10.1016/j.margeo.2012.07.013

Schmidely, L., Nehrbass-Ahles, C., Schmitt, J., Han, J., and Stocker, T. F. (2021). CH4 and N2O Fluctuations During the Penultimate Deglaciation. *Clim. Past.* 17 (4), 1627–1643. doi: 10.5194/cp-17-1627-2021

Schmidt, H., Berger, W. H., Bickert, T., and Wefer, G. (1993). Quaternary Carbon Isotope Record of Pelagic Foraminifers: Site 806, Ontong Java Plateau. *Proc. Ocean Drill. Prog. Sci. Results.* 130, 397–409. doi: 10.2973/odp.proc.sr.130.024.1993

Scholz, F., Hensen, C., Noffke, A., Rohde, A., Liebetrau, V., and Wallmann, K. (2011). Early Diagenesis of Redox-Sensitive Trace Metals in the Peru Upwelling Area Response to ENSOrelated Oxygen Fluctuations in the Water Column. *Geochim. Cosmochim. Ac.* 75, 7257–7276. doi: 10.1016/j.gca.2011.08.007

Scholz, F., Siebert, C., Dale, A. W., and Frank, M. (2017). Intense Molybdenum Accumulation in Sediments Underneath a Nitrogenous Water Column and Implications for the Reconstruction of Paleo-Redox Conditions Based on Molybdenum Isotopes. *Geochim. Cosmochim. Ac.* 213, 400–417. doi: 10.1016/j.gca.2017.06.048

Scott, C., and Lyons, T. W. (2012). Contrasting Molybdenum Cycling and Isotopic Properties in Euxinic Versus Non-Euxinic Sediments and Sedimentary Rocks: Refining the Paleoproxies. *Chem. Geol.* 324-325, 19–27. doi: 10.1016/j.chemgeo.2012.05.012

Serov, P., Vadakkepuliyambatta, S., Mienert, J., Patton, H., Portnov, A., Silyakova, A., et al. (2017). Postglacial Response of Arctic Ocean Gas Hydrates to Climatic Amelioration. *Proc. Natl. Acad. Sci. U. S. A.* 114, 6215–6220. doi: 10.1073/pnas.1619288114

Shackleton, N. J., and Hall, M. A. (1989). Stable Isotope History of the Pleistocene at ODP Site 677. *Ocean Drill. Prog. Sci. Results.* 111, 295–316. doi: 10.2973/odp.proc.sr.111.150.1989

Shakhova, N., Semiletov, I., Salyuk, A., Yusupov, V., Kosmach, D., and Gustafsson, O. (2010). Extensive Methane Venting to the Atmosphere From Sediments of the East Siberian Arctic Shelf. *Science* 327, 1246–1250. doi: 10.1126/science.1182221

Sluijs, A., Brinkhuis, H., Schouten, S., Steven, M. B., Cédric, M. J., James, C. Z., et al. (2007). Environmental Precursors to Rapid Light Carbon Injection at the Palaeocene/Eocene Boundary. *Nature* 450, 1218–1221. doi: 10.1038/nature06400

Smrzka, D., Feng, D., Himmler, T., Zwicker, J., Hu, Y., Monien, P., et al. (2020). Trace Elements in Methane-Seep Carbonates: Potentials, Limitations, and Perspectives. *Earth Sci. Rev.* 208, 103263. doi: 10.1016/j.earscirev.2020.103263

Svensen, H. (2012). Bubbles From the Deep. *Nature* 483 (7390), 413–415. doi: 10.1086/629067

Taylor, S. R., and McLennan, S. M. (1985). The Continental Crust: Its Composition and Evolution. *J. Geol.* 94, 57–72.

Tong, H., Feng, D., Cheng, H., Yang, S., Wang, H., Min, A. G., et al. (2013). Authigenic Carbonates From Seeps on the Northern Continental Slope of the South China Sea: New Insights Into Fluid Sources and Geochronology. *Mar. Pet. Geol.* 43, 260–271. doi: 10.1016/j.marpetgeo.2013.01.011

Wang, S., Magalhaes, V. H., Pinheiro, L. M., Liu, J., and Yan, W. (2015). Tracing the Composition, Fluid Source and Formation Conditions of the Methane-Derived Authigenic Carbonates in the Gulf of Cadiz With Rare Earth Elements and Stable Isotopes. *Mar. Petrol. Geol.* 68, 192–205. doi: 10.1016/j.marpetgeo.2015.08.022

Wei, J., Liang, J., Lu, J., Zhang, W., and He, Y. (2019). Characteristics and Dynamics of Gas Hydrate Systems in the Northwestern South China Sea - Results of the Fifth Gas Hydrate Drilling Expedition. *Mar. Petrol. Geol.* 110, 287–298. doi: 10.1016/j.marpetgeo.2019.07.028

Wei, J., Wu, T., Zhang, W., Deng, Y., Xie, R., Feng, J., et al. (2020). Deeply Buried Authigenic Carbonates in the Qiongdongnan Basin, South China Sea: Implications for Ancient Cold Seep Activities. *Minerals* 10 (12), 1135. doi: 10.3390/min10121135

Wignall, P. B., and Twitchett, R. J. (1996). Oceanic Anoxia and the End Permian Mass Extinction. *Science* 272, 1155–1158. doi: 10.1126/science.272.5265.1155

Yang, K., Chu, F., Zhu, Z., Dong, Y., Yu, X., Zhang, W., et al. (2018). Formation of Methane-Derived Carbonates During the Last Glacial Period on the Northern Slope of the South China Sea. *J. Asian Earth Sci.* 168, 173–185. doi: 10.1016/j.jseaes.2018.01.022

Ye, J., Wei, J., Liang, J., Lu, J., Lu, H., and Zhang, W. (2019). Complex Gas Hydrate System in a Gas Chimney, South China Sea. *Mar. Petrol. Geol.* 104, 29–39. doi: 10.1016/j.marpetgeo.2019.03.023